JACS
JOURNAL OF THE AMERICAN CHEMICAL SOCIETY
Article
pubs.acs.org/JACS

Stabilizing Lithium Metal Anodes by Uniform Li-Ion Flux Distribution in Nanochannel Confinement

Wei Liu,[†,§] Dingchang Lin,[†,§] Allen Pei,[†,§] and Yi Cui*[,†,‡]

[†]Department of Materials Science and Engineering, Stanford University, Stanford, California 94305, United States
[‡]Stanford Institute for Materials and Energy Sciences, SLAC National Accelerator Laboratory, 2575 Sand Hill Road, Menlo Park, California 94025, United States

Supporting Information

ABSTRACT: The widespread implementation of high-energy-density lithium metal batteries has long been fettered by lithium dendrite-related failure. Here we report a new strategy to address the issue of dendrite growth by a polyimide-coating layer with vertical nanoscale channels of high aspect ratio. Smooth, granular lithium metal was deposited on the modified electrode instead of typical filamentary growths. In a comparison with the bare planar electrode, the modified electrode achieved greatly enhanced Coulombic efficiency and longer cycle life. Homogeneous Li^+ flux distribution above the modified electrode from the nanochannel confinement can account for a uniform Li nucleation and a nondendrite growth. We also demonstrated that the polyimide coating with microscale pores loses the confinement effects and fails to suppress lithium dendrites. This strategy of spatially defined lithium growth in vertical-aligned nanochannels provides a novel approach and a significant step toward stabilizing Li metal anodes.

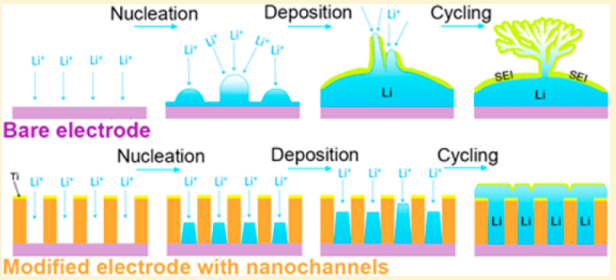

INTRODUCTION

Technological improvements in high-energy-density rechargeable batteries are being driven by an ever-increasing demand for portable electronic devices, electrical transportation, as well as grid-scale energy storage. Intense research has been focused on high specific capacity battery chemistries. Anodes include Si, Ge, Sn, and Li metal,[1−4] and cathodes include sulfur[5] as well as air.[6] Li metal is an attractive anode material, possessing a high theoretical specific capacity (3860 mAh g^{-1} compared to 372 mAh g^{-1} for the widely used graphite anode in Li-ion batteries), low density (0.534 g cm^{-3}), and the lowest electrochemical potential (−3.040 V versus standard hydrogen electrode).[7−10] Unfortunately, issues with safety and efficiency that emerge during prolonged battery operation prevent metallic lithium from being used in commercialized Li metal batteries. Upon repeated Li deposition/dissolution processes, the surface of the Li metal anode uncontrollably develops dendritic growths that can penetrate the separator and form an internal short to the cathode, initiating a thermal runaway reaction and catastrophic battery failure. The Li dendrite-electrolyte interface with high surface area facilitates the reaction and formation of solid-electrolyte-interphase (SEI) layers on the Li surface, leading to corrosion and isolation of Li, consequently resulting in increased interfacial resistance due to the thick SEI and a fast loss in Coulombic efficiency (CE).[11,12]

Accordingly, several approaches for modifying the morphology of the electroplated Li have been adopted with varying degrees of success for suppressing dendritic growth and improving cycling efficiency. One method is to control the Li metal/electrolyte interface with protective layers. Zheng et al.[13] proposed a coating layer of hollow carbon nanospheres to successfully inhibit the growth of lithium dendrites. Two-dimensional (2D) boron nitride[14] and graphene[15] have also been utilized as chemically and physically stable barriers on Li metal. In addition, the use of solid-state electrolytes including polymer membranes[16,17] and especially ceramic electrolytes[18,19] has been shown to be effective for suppressing the growth of lithium dendrites. However, low ionic conductivity and large interfacial resistance limit the wide use of solid electrolytes. Although the protective coating method can enhance compatibility between the lithium anode and electrolyte, the intrinsic problem of uneven lithium electrodeposition remains unsolved. Furthermore, various electrolyte additives have been explored to suppress dendrite growth and reinforce the lithium surface, including vinylene carbonate,[20] Cs^+ and Rb^+,[21] LiF,[22,23] lithium polysulfide,[24] and ionic liquids.[25] However, stable cycling over long periods of time cannot be guaranteed due to consumption of the additives. Moreover, for Li metal anode, Li deposition/dissolution processes take place without a host material, unlike the graphite anode that has only 10% volume change during lithiation. So the "hostless" nature of Li metal with its virtually infinite relative volume change during cycling and without a material host for atom insertion was recognized as a major root cause in recent studies.[26−30] Various rational designs of a "host" have been demonstrated including hollow

Received: August 24, 2016
Published: November 2, 2016

DOI: 10.1021/jacs.6b08730
J. Am. Chem. Soc. 2016, 138, 15443−15450

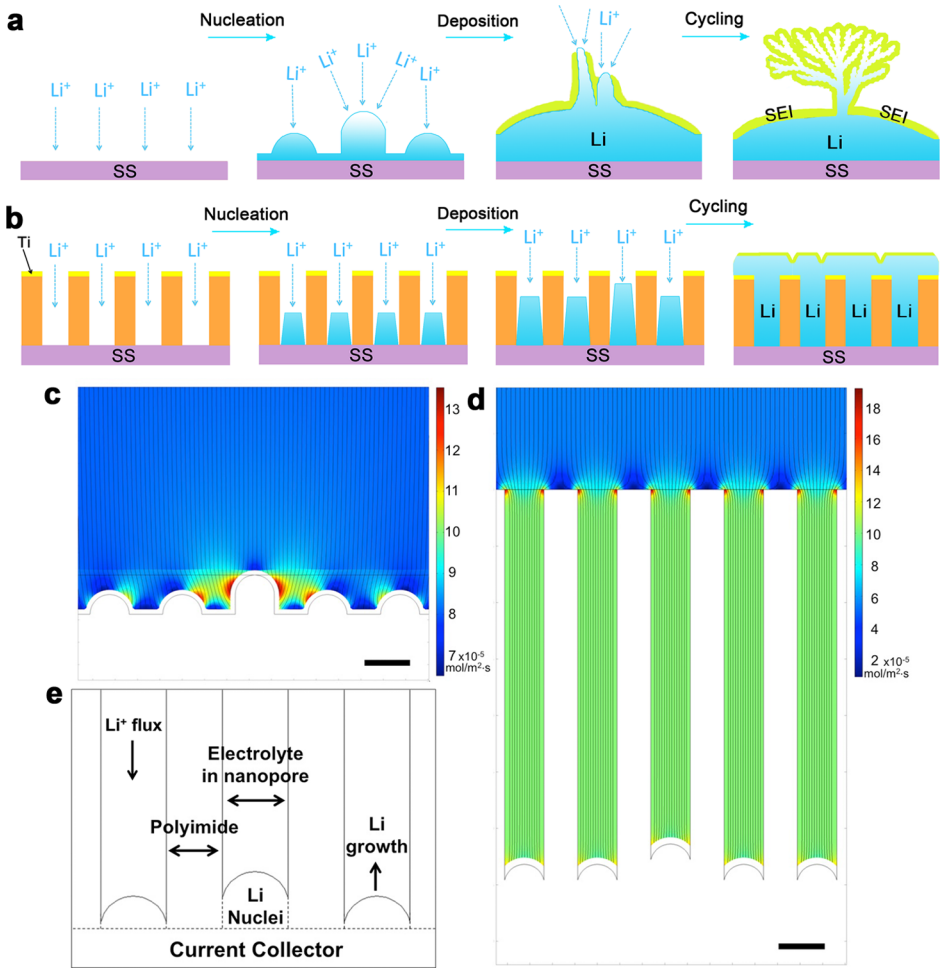

Figure 1. Schematic diagrams for the comparison of Li anodes with and without the vertical-aligned nanochannel coating and simulation of Li^+ flux during deposition on the two electrodes. (a) For bare electrode, volumetric changes during the Li deposition process can easily break the SEI layer. This behavior leads to concentration of Li^+ flux near cracks, pits, and crevices, and consequently ramified growth of Li dendrites and rapid consumption of the electrolyte. (b) A modified SS electrode coated with a nanochannel layer creates confinements for Li deposition showing uniform nucleation and growth due to equal Li^+ flux in each nanoscaled pore, which results in nondendritic Li. The volumetric expansion of the Li deposition process is also partially negated within the volume of the pores due to the fixed thickness of the membrane. (c) Simulation for the bare electrode. Li^+ flux is seen to be greatly enhanced near protruding nonuniform Li nuclei, generating hot spots for Li dendrite formation. Flux streamlines are obviously converging near the taller nuclei, resulting in further amplified Li growth. (d) In the case of the electrode with the nanochannel coating of 3.5 μm in height, Li^+ flux is evenly distributed within the pores, indicating the homogenizing effect of the coating structure. At the bottom of the nanochannel, a lack of hot spots is apparent at the Li surface, even near the protruding nuclei. (e) Simulation cell geometry for the case with nanochannel coating. Scale bars: 400 nm.

carbon spheres,[26] graphene oxides,[27] carbon[28] and polymer nanofibers,[29] and porous Cu.[30] A concept of "lithiophilic" surface for wetting of lithium metal was proposed.[27−29] The host scaffold with lithiophilic coating could allow complete lithium entrapment.

Additionally, various approaches based on nanopores polymer/ceramic separators/electrolytes have been demonstrated to effectively improve the stability of lithium deposition.[23,31−36] Archer group reported a composite nanoporous alumina/PVDF separator that could stabilize electrodeposition in lithium metal batteries and improve its lifetime greatly.[23,31] Recently, Bazant's group demonstrated that the anodic aluminum oxide (AAO) membrane with pores smaller than mossy lithium whiskers could enhance safety and cycle life by replacing polyolefin separators.[33]

Herein, the present work demonstrates a distinct, novel approach to suppress Li dendrites at a fundamental level via manipulating Li^+ flux homogeneous distribution above the anode through nanoscaled confinement, resulting in a uniform Li nucleation and growth. As shown in Figure 1a, dendritic Li growth is expected from bare planar electrodes. Volumetric changes during the Li deposition/dissolution process can easily break the SEI layer, which leads to concentration of Li^+ flux near cracks, pits, and crevices and consequent ramified Li filamentary growths and rapid consumption of the electrolyte with reduced CE. In contrast, as proposed in Figure 1b, uniform Li deposition without mossy-like morphology is expected for the modified electrode coated with a thin polymer layer with vertical-aligned nanochannels. The nanosized channels with high aspect ratio are able to divide the space above the anode into small confinements, so that Li-ions could prefer to move along the normal direction of the electrode rather than the parallel direction. That means that even though the height of one Li deposit in one channel is more than the others, the Li^+ flux near this Li deposit could not be amplified uncontrollably since the flux in each nanochannel is confined

DOI: 10.1021/jacs.6b08730
J. Am. Chem. Soc. 2016, 138, 15443−15450

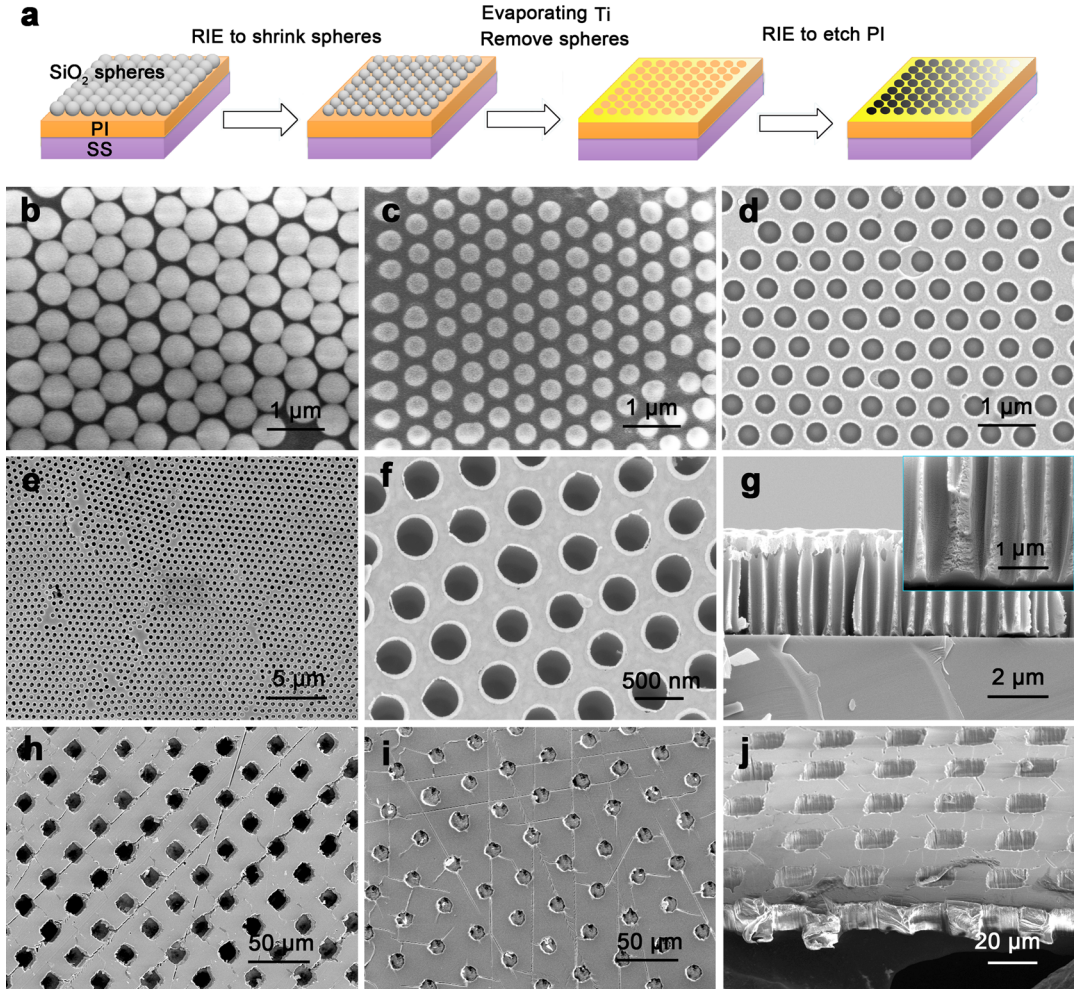

Figure 2. Fabrication process and micromorphologies of the PI membrane with vertical-aligned nano- and microsized channels. (a) Schematic illustration for the fabrication of the modified electrode with PIANC coating. (b) SEM image of silica nanosphere monolayer on the PI with SS substrate. (c) Shrunk silica nanospheres by RIE based on fluorine chemistry using CHF_3. (d) SEM image of the Ti mask with nanoscale holes. SEM images of the PI membrane with vertical nanopores on SS substrate at (e) low and (f) high magnification. (g) Cross sectional view of the PIANC coating. SEM image of top view for the PIAMC membrane, showing (h) square and (i) circle shape, and (j) cross sectional SEM image.

and isolated from each other. Hence, the magnitude of Li^+ flux in each nanochannel could be relatively homogeneous during Li deposition, resulting in a uniform nucleation and growth, and the Li deposit could not grow into elongated metal filaments like the bare electrode. Meanwhile, the volumetric expansion of the Li deposition can also be partially negated within the volume of the pores due to the fixed thickness of the coating. Additionally and importantly, the porous polymer membrane contacted with the current collector tightly, which avoids the possibility of its lift up by the deposition of Li metal.

RESULTS AND DISCUSSION

Simulation Analysis. To visualize the Li^+ flux during Li deposition in the vertical-aligned nanochannels, we created a simulation cell emulating our experimental setup in COMSOL. It is well-known that nonuniformities including protrusions and SEI cracks on the Li surface will be amplified during growth, resulting in ramified dendritic lithium, which is detrimental to electrode performance.[9,11] In our simulation, we compared the ionic flux and local current densities for two different electrode geometries: planar electrodes with and without nanochannel coatings. For the bare planar electrode, a uniform array of hemispherical Li nuclei with diameter 350 nm (to match the size of the nanoscaled pores) was initially generated on a planar current collector. One nucleus was extended vertically to double the height of the other nuclei, representing a nonuniformity that could arise from fluctuations in the cell environment. Lithium deposition was carried out for 200 s, and the magnitude and direction of Li^+ flux were plotted. Figure 1c depicts the ionic flux around the nuclei for the control electrode geometry where no nanopores are present. Regions of increased Li^+ flux (nearly double of that within the bulk electrolyte), also known as "hot spots", are clearly visible in red near the protruding nuclei and can promote dendrite formation and SEI breakage. Additionally, the plotted streamlines indicate the direction of Li^+ flux; the streamlines in the entire cell converge toward the larger nuclei, indicating the possibility of rapid self-amplified growth. Conversely, in Figure 1d, when the nanochannel coating is introduced into the electrode geometry, the ionic flux streamlines are seen to be more uniformly distributed within the columnar pores. The current density in the channel with the protruding nuclei is only increased by 0.18% relative to that of the surrounding channels, demonstrating that the nanochannel coating effectively homogenizes and screens any perturbations to the Li deposition process. At the Li nuclei surfaces, no hotspots are visible, indicating that

DOI: 10.1021/jacs.6b08730
J. Am. Chem. Soc. 2016, 138, 15443−15450

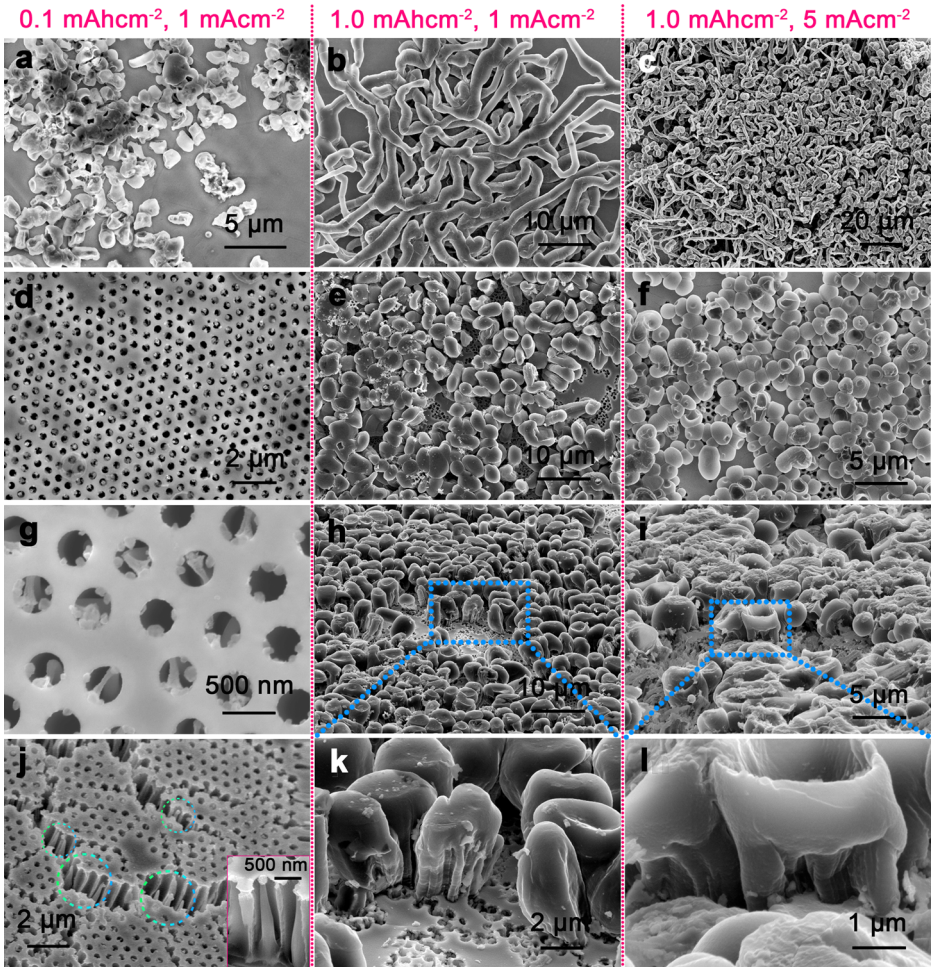

Figure 3. Morphology study of Li deposition on SS electrode with and without PIANC coating. SEM images of lithium metal deposited on a bare SS substrate at current densities and deposition capacities of (a) 1 mA cm^{-2} and 0.1 mAh cm^{-2}, (b) 1 mA cm^{-2} and 1.0 mAh cm^{-2}, and (c) 5 mA cm^{-2} and 1.0 mAh cm^{-2}, respectively. Top view and cross sectional SEM images with various magnifications of lithium metal deposited on modified electrode at current densities and deposition capacities of (d, g, j) 1 mA cm^{-2} and 0.1 mAh cm^{-2}, (e, h, k) 1 mA cm^{-2} and 1.0 mAh cm^{-2}, and (f, i, l) 5 mA cm^{-2} and 1.0 mAh cm^{-2}, respectively.

significant deviations in Li^+ flux magnitude are suppressed. Figure 1e shows a schematic of the structure of the simulation cell seen in Figure 1d for clarity. Additional simulations and parameters are available in Supporting Information Figure S1. Moreover, in order to fabricate the porous polymer membrane with appropriate and effective thickness to suppress Li dendrite, simulations of the effects of varying the height of nanochannels were studied. As shown in Supporting Information Figure S2, it demonstrates that the coating with 1 μm height of nanochannels is too short to have the flux-smoothing effects present for longer channels (3.5 and 10 μm). As such, the nanochannels with thickness of about 3.5 μm and large aspect ratio of 10 were chosen in the current work.

Morphological and Structural Analysis. Polyimide (PI) is endowed with good chemical and physical stability in battery environments and as a result is a promising candidate coating material.[29,37] Therefore, we fabricated a PI coating with aligned nano- and microsized channels (defined as PIANC and PIAMC coating) on stainless steel (SS) for stabilizing Li deposition. As the typical diameter of lithium dendrites is around 2 μm for ether-based electrolyte,[13,33] two representative pore sizes have been investigated in the present work, including 350 nm diameter (nanoscaled pore) and 15 μm (microscaled pore), to see how the lithium depositions take place. The fabrication process for the PIANC coating is illustrated in Figure 2a. A uniform PI membrane was first coated on the SS substrate using a doctor blade. Monodisperse silica nanospheres were then assembled into a close-packed monolayer on the PI coating using the Langmuir–Blodgett (LB) method, as shown in Figure 2b. The diameter and spacing of the silica nanoparticles are readily tuned by selective and isotropic reactive-ion etching (RIE), which enables various pore sizes and porosities. In the current work, initial silica nanoparticles of diameter 550 nm were etched to a final diameter of 350 nm, resulting in an areal porosity of 36%. Figure 2c,d shows the shrunk nanospheres of 350 nm diameter and the Ti mask with nanoholes, respectively. The PI membrane with vertical channels was obtained by reactive-ion etching (RIE) using a mix of O_2 and N_2 gas (Figure 2e–g). As demonstrated in the cross sectional SEM in Figure 2g, the straight channels in the PI layer are clearly observed. For the PI coating with microsized pores (15 μm) (Figure 2h–j), the Ti micropatterned mask on the PI membrane was fabricated by typical photolithography. Both square- and circle-shaped pores were prepared. The thickness of the PIAMC coating is 15–20 μm. It can be seen that this multistep coating process to fabricate nano-/microsized-aligned pores could be applied on various electrode

DOI: 10.1021/jacs.6b08730
J. Am. Chem. Soc. 2016, 138, 15443–15450

materials, based on the mature and flexible techniques including LB coating, photolithography, and RIE process.

Morphology of Lithium Metal Deposition. Lithium metal deposition/dissolution was investigated using a two-electrode configuration composed of a Li metal electrode versus an SS foil assembled in coin cells. 1.0 M LiTFSI in 1:1 v/v DOL/DME with 1 wt % $LiNO_3$ was used if no clarification of electrolyte is given. The confinement effect of the PIANC coating was systematically investigated by varying the amount of Li deposited galvanostatically onto the SS electrode and observing the morphology of the resulting Li metal deposits. Figure 3a–c clearly shows the direct deposition of Li metal onto a bare SS electrode at various current densities and deposition capacities. For a small amount of lithium metal deposition (0.1 mAh cm^{-2}), uniform spherical nuclei of Li particles without any filaments or wire-like growths could be seen. The nuclei size can be seen in Figure 3a with an average size of 1.6 μm, which is in agreement with reported results.[13,33] However, with additional plating of lithium metal to a capacity of 1.0 mAh cm^{-2}, a typically ragged growth of elongated lithium deposits could be formed. The tilted-view SEM image shown in Supporting Information Figure S3 also clearly shows the dendritic morphology for the deposited lithium metal. During lithium deposition, electrons prefer to accumulate at the ridges or tips with microscopic roughness and promote lithium metal deposition at those spots from incoming Li^+ ions in the electrolyte.[38]

On the basis of our simulation results, we expect that spatial control of Li^+ ion motion may be a promising strategy to stabilize dendritic growth dynamics, achieved here by the division of the working electrode surface into small compartments for Li plating. The nucleation and growth of Li confined in pores can result in significantly different morphologies compared to bare planar electrodes, particularly when the pore dimensions are smaller than the critical size of an emergent nucleus.[39] To understand the evolution of Li deposition on the SS electrode coated with a PIANC layer, *ex situ* SEM images of Li metal deposited at various current densities and deposition capacities have been carried out, as shown in the SEM images of Figure 3d–l. At the initial stage of Li deposition with a capacity of 0.1 mAh cm^{-2} at a current density of 1 mA cm^{-2}, one lithium nanopillar in one nanochannel that does not protrude out of the surface of the PI coating is observed to grow from the center of the pores (Figure 3d,g,j), which indicates uniform Li nucleation. Further deposition of Li metal on the modified SS electrode to 1.0 mAh cm^{-2} shows Li with a columnar, smooth, rounded morphology instead of a typical sharp filamentary shape on the PI surface (Figure 3e,h,k), which is in an agreement with what we proposed and the simulation results. It can be seen clearly from Figure 3h,l that although the Li metal pillars protrude out of the PIANC coating, they merged into large granules with rounded edges. Even for an extremely high current density of 5 mA cm^{-2} (Figure 3f,i,l), the deposited Li metal also has a columnar structure rather than dendritic morphology. According to the literature,[33,40,41] lithium metal mainly grows from its roots below the limiting current density. In the current study, the current density is in the low-current-density regime, so the Li growth may take place from the roots. In this case, even when the capacity of the deposited Li metal is more than that which can be confined in the pores, the homogeneous distribution of Li-ion flux above the modified electrode still could be confined by the nanochannels, which results in the flat lithium deposition at higher deposited capacity and the improved CE shown in the following study. However, at much higher deposited capacities (3–5 mAh cm^2) needed in practical batteries, larger aspect ratios for the aligned pores are required. The current densities used in the current work are in the range 1–5 mA cm^{-2}, in the low-current-density regime that is insufficient to cause mass-transport-limited dendritic deposition within the pores.[33,42] However, uneven lithium deposits could be also observed in the form of elongated metal filaments, which is in agreement with reported results.[43,44] It is worth noting that while altering the porosity and pore sizes of the membrane will change the effective current density within the pores, the limiting current density cannot be surpassed even for extremely low porosities of only 1%, as shown in Supporting Information Figures S4 and S5.

The morphology of the deposited lithium metal after 200 plating/stripping cycles is shown in Supporting Information Figure S6, showing a compact, nonporous, and uniform bulk of Li metal without any protruding filaments. Furthermore, this PIANC coating remains structurally stable after Li stripping (Supporting Information Figure S7). While SEM images can show the morphologies of lithium filaments, it cannot provide Li deposition in real time and with quantitative information. Nuclear magnetic resonance (NMR) spectroscopy is a powerful technique to indicate time-resolved and quantitative results on lithium metal structure and growth during battery operation.[45−47] As such, ^{7}Li solid-state NMR carried out in the next investigation could provide more detailed evidence of Li morphology improvement during intermediate states of deposition. It is also worth noting that, besides the morphology of nanochannels, the coating material (PI) may also influence lithium metal deposition. However, the coating material of PI is one of the few polymers that exhibit high performance in battery environments, including good chemical stability and physical stability at high temperatures.[29,37] In addition, due to the electrically insulating nature of the porous PI coating, lithium plating is confined within the nanochannels rather than on the PI surface.[29] Thus, the effects of the coating material PI on lithium deposition are expected to be minimal due to its inertness. Therefore, these exciting results support the hypothesis of suppressed Li dendrite growth by coating PIANC on the electrode. The nanochannels with high aspect ratio can effectively "screen" morphology-induced electric field imbalances (Figure 1b), resulting in uniform nucleation and subsequently even Li deposition/dissolution controlled by a fairly homogeneous Li^+ flux in each channel.

Electrochemical Testing. Galvanostatic Li deposition and dissolution cycling were carried out to substantiate the practicality of the modified electrode coated with PIANC and its chemical stability in contact with Li metal. Coin cells were assembled using lithium foil as the counter-electrode and SS foil as the working electrode to study the cycling stability and CE of Li plating/stripping. CE was defined as stripping capacity over deposition capacity. The results are shown in Figure 4, plotted as the CE versus cycle number of the cells at various current densities with the same areal capacities of 0.5 mAh cm^{-2}. In comparison to the bare SS electrode, the modified electrode with PIANC coating demonstrated more stable electrochemical cycling and a longer cell life. At current densities of 1.0, 2.0, and 3.0 mA cm^{-2}, the cells with modified electrodes exhibited significantly improved CE of 97.6% over 240 cycles, 92.9% over 150 cycles, and 88.6% over 140 cycles, respectively. In sharp contrast, the cells using bare SS electrode showed rapid decay

DOI: 10.1021/jacs.6b08730
J. Am. Chem. Soc. 2016, 138, 15443−15450

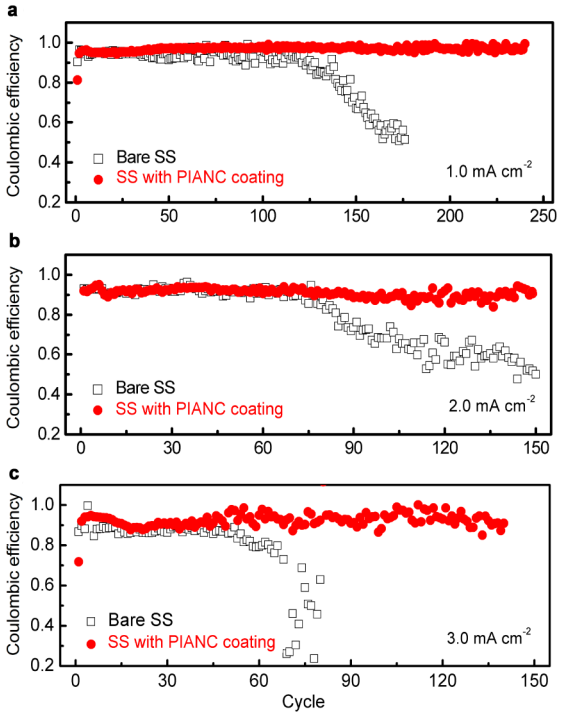

Figure 4. Electrochemical characterization of the electrodes with PIANC coating for Li deposition/dissolution, together with the data for the bare SS electrode. Comparison of CE of Li deposition/stripping with and without PIANC coating at various current rates of (a) 1.0, (b) 2.0, and (c) 3.0 mA cm^{-2} with the same areal capacities of 0.5 mAh cm^{-2}.

after 125, 75, and 50 cycles, respectively. Additionally, Supporting Information Figure S8 illustrates the CE versus cycle number of the cells at various deposited areal capacities in the range 0.5–2.0 mAh cm^{-2} and at the same current density of 1.0 mA cm^{-2}, which also indicates much improved CE and cycle life for the cells using PIANC-modified electrodes. The capacity decay with cycling can be explained by the formation of SEI due to consumption of electrolyte and by "dead" Li detached from the current collector. The fixed confined space could contribute there to formation of a more stable SEI layer, which improves CE. Hence, as shown in Figure 1b, the space upon the negative electrode is divided into nanosized confinements (350 nm) by the use of PIANC coating, which results in a relatively equal concentration of Li^+ ion flux in each nanochannel. Therefore, an even Li nuclei distribution and a uniform Li growth in each nanochannel are expected, which contribute to the stabilization of Li metal anode. Because of the improved Li^+ flux uniformity and structural protection of the "roots" of the Li metal growths in the coated electrodes, there may be less dead Li present after cycling. Therefore, the high CE for Li deposition and stripping after 1 mAh cm^{-2} of Li capacity was achieved. By using the PIANC coating, partially fixed volume expansion could also be achieved. Moreover, Supporting Information Figure S9 indicates that the electrochemical performance of the Li/$LiFePO_4$ full cell was also improved by the use of nanochannel coating.

Furthermore, AC impedance spectroscopy analysis of the cells using the SS electrode coated with PIANC layer was performed to gain insight into the growth of Li metal. Figure 5a shows the impedance spectroscopy for the pristine cells using the bare SS electrode and the modified electrode with a PIANC coating. In the equivalent circuit, R_1 is the electrolyte resistance and contact resistances from electrode leads and terminals. R_2 and R_3 correspond to the current collector/electrolyte interface and Li/electrolyte interface, respectively. CPE1 and CPE2 are the constant phase elements to fit capacitances. The spike at low frequencies is due to an ion diffusion-limited process contributing to the Warburg impedance Z_w response.[48] These two types of electrodes were observed to have similar electrolyte resistance, interfacial resistance, and total resistance, as seen in Figure 5a. It is noteworthy that at low frequencies the slope for the PIANC coated SS is larger than that for bare SS (Figure 5a), which implies an increased diffusive behavior by using the interfacial layer of aligned porous PI coating. Figure 5b plots the impedance spectroscopy for a bare SS electrode and a modified electrode after various Li plating/stripping cycles. After cycles, a curved line instead of a straight line is shown at low frequencies (Figure 5b), which indicates more activated interfacial charge-transfer process and electrochemical reactions that occur at the electrode surface. It also can be seen that the electrolyte resistance and the interfacial resistance increase with the cycle number for both cells due to the consumption of electrolyte and the formation of the SEI layer. Compared with the cell using bare SS electrode, the cell using a PIANC-modified electrode showed much smaller increases in resistances, which is in agreement with the CE performance from cycling tests that the nanoconfinement guaranteed more uniform Li deposition, more stable SEI formation, and consequently a better cycling stability.

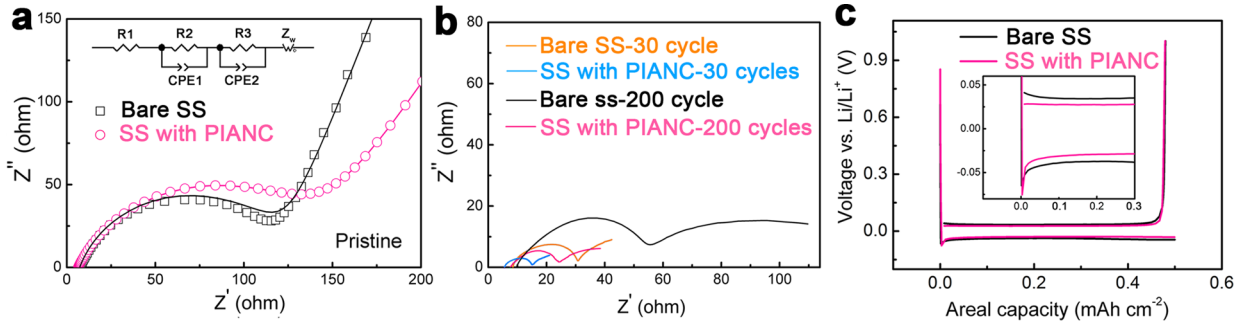

Figure 5. Impedance spectra study of the electrodes with or without coating for Li deposition/dissolution. (a) Experimental and fitted impedance spectra for the pristine cells using the electrodes with PIANC coating, and using the bare electrode. The inset is the equivalent circuit. (b) Impedance spectra for the cells using the modified electrodes with PIANC compared with the bare electrode after 30 and 200 cycles. (c) Voltage profiles of the Li deposition/dissolution process with Li metal as the reference/counter-electrode at 1.0 mA cm^{-2} for the bare electrode and modified electrode.

DOI: 10.1021/jacs.6b08730
J. Am. Chem. Soc. 2016, 138, 15443–15450

However, when the size of the vertical channel increases to the microscale (15 μm), the growth of dendritic lithium could not be suppressed, as shown in Supporting Information Figure S10. The thickness of the PIAMC coating is about 15 μm. With the deposition of Li metal, the pores were gradually filled with filamentary Li deposits. The Li deposits prefer to grow along the wall of the microscaled channels, which results in reduced surface area that is exposed to electrolyte. Subsequently, electrodes coated with a PIAMC layer exhibit enhanced stable cycling efficiency compared with the cells using the bare SS foil, as shown in Supporting Information Figure S11. However, the PIANC coating still out-performs the PIAMC coating due to the spatial confinement effects discussed previously, although the resistance for the pristine cells using modified electrode with PIAMC coating is not much increased (Supporting Information Figure S12).

Additionally, the morphologies of Li metal deposited from $LiPF_6$ in EC/DEC electrolyte were also characterized. Supporting Information Figure S13 shows the SEM image of Li plated at a current density of 1.0 mA cm^{-2} and capacity of 0.5 mAh cm^{-2} on bare SS electrode, exhibiting needle-like lithium dendrites with the diameter of around 200 nm. In contrast, a homogeneous confined growth of Li metal in nanosized pores was observed on the SS electrode coated with the PIANC layer. However, similar to the case in ether-based electrolyte, microsized channels could not suppress the growth of lithium dendrites, as shown in Supporting Information Figure S13e,f. The cycling performance for the modified electrode with nanochannels using carbonate electrolytes is shown in Supporting Information Figure S14, which indicates more stable CE.

CONCLUSIONS

In summary, the present work appears to be the first demonstration of the electrochemical deposition of Li metal in a vertical-aligned porous structure. PI membranes with vertical nano- and microsized channels have been successfully fabricated on the SS electrode. The results reveal that Li metal is accommodated in the pores on the modified electrode at low deposited capacity, while smooth, granular Li metal protrudes on the surface without the formation of elongated metal filaments when the capacity of the pores is exceeded. Compared with using bare electrode, the lithium metal cell using the electrode coated with nanochannels demonstrated enormously enhanced CE and longer cycle life. A relatively equal Li^+ flux in each nanochannel with large aspect ratio contributes to a homogeneous Li nuclei distribution and growth is expected, which results in the stabilization of the Li metal anode. Meanwhile, the microsized confinement is almost ineffectual for suppressing Li dendrites. This unique nano-architecture makes a significant step toward stabilizing lithium metal anodes. More efforts need to be devoted to enable stable cycling even at high current densities and commercial-level areal capacities in Li metal-based batteries, such as Li–air and Li–sulfur, for next generation energy storage devices. More importantly, this coating process to fabricate nano/microsized-aligned pores can be easily scaled up without complicated procedures at low cost and high efficiency in terms of applicability.

ASSOCIATED CONTENT

Supporting Information

The Supporting Information is available free of charge on the ACS Publications website at DOI: 10.1021/jacs.6b08730.

Complete experimental details and additional characterizations (PDF)

AUTHOR INFORMATION

Corresponding Author

*E-mail: yicui@stanford.edu.

Author Contributions

§W.L., D.L., and A.P. contributed equally to this work.

Notes

The authors declare no competing financial interest.

ACKNOWLEDGMENTS

This work is supported by Samsung Electronics.

REFERENCES

(1) Sun, Y.; et al. *Nature Eng.* **2016**, *1*, 16071.
(2) Chan, C. K.; et al. *Nat. Nanotechnol.* **2008**, *3*, 31–35.
(3) Chan, C. K.; Zhang, X. F.; Cui, Y. *Nano Lett.* **2008**, *8*, 307–309.
(4) Derrien, G.; et al. *Adv. Mater.* **2007**, *19*, 2336–2340.
(5) Yang, Y.; Zheng, G.; Cui, Y. *Chem. Soc. Rev.* **2013**, *42*, 3018–3032.
(6) Bruce, P. G.; Freunberger, S. A.; Hardwick, L. J.; Tarascon, J.-M. *Nat. Mater.* **2012**, *11*, 19–29.
(7) Tarascon, J. M.; Armand, M. *Nature* **2001**, *414*, 359–367.
(8) Kim, H.; et al. *Chem. Soc. Rev.* **2013**, *42*, 9011–9034.
(9) Xu, W.; et al. *Energy Environ. Sci.* **2014**, *7*, 513–537.
(10) Tikekar, M. D.; et al. *Nature Energy* **2016**, *1*, 16114.
(11) Chazalviel, J.-N. *Phys. Rev. A: At., Mol., Opt. Phys.* **1990**, *42*, 7355.
(12) Bhattacharyya, R.; et al. *Nat. Mater.* **2010**, *9*, 504–510.
(13) Zheng, G.; et al. *Nat. Nanotechnol.* **2014**, *9*, 618–623.
(14) Yan, K.; et al. *Nano Lett.* **2014**, *14*, 6016–6022.
(15) Kim, J. S.; et al. *Chem. Mater.* **2015**, *27*, 2780–2787.
(16) Croce, F.; et al. *Nature* **1998**, *394*, 456–458.
(17) Liu, W.; et al. *Nano Lett.* **2015**, *15*, 2740–2745.
(18) Fergus, J. W. *J. Power Sources* **2010**, *195*, 4554–4569.
(19) Kamaya, N.; et al. *Nat. Mater.* **2011**, *10*, 682–686.
(20) Ota, H.; et al. *Electrochim. Acta* **2004**, *49*, 565–572.
(21) Ding, F.; et al. *J. Am. Chem. Soc.* **2013**, *135*, 4450–4456.
(22) Kanamura, K.; Shiraishi, S.; Takehara, Z. *J. Electrochem. Soc.* **1996**, *143*, 2187–2197.
(23) Lu, Y.; Tu, Z.; Archer, L. A. *Nat. Mater.* **2014**, *13*, 961–969.
(24) Li, W. *Nature Commun.* **2015**, *6*, 7436.
(25) Grande, L.; et al. *ACS Appl. Mater. Interfaces* **2015**, *7*, 5950–5958.
(26) Yan, K.; et al. *Nature Eng.* **2016**, *1*, 16010.
(27) Lin, D.; et al. *Nat. Nanotechnol.* **2016**, *11*, 626–632.
(28) Liang, Z.; et al. *Proc. Natl. Acad. Sci. U. S. A.* **2016**, *113*, 2862–2867.
(29) Liu, Y. *Nature Commun.* **2016**, *7*, 10992.
(30) Yun, Q.; et al. *Adv. Mater.* **2016**, *28*, 6932–6939.
(31) Tu, Z.; Kambe, Y.; Lu, Y.; Archer, L. A. *Adv. Energy Mater.* **2014**, *4*, 1300654.
(32) Tu, Z.; Lu, Y.; Archer, L. *Small* **2015**, *11*, 2631–2635.
(33) Bai, P.; et al. *Energy Environ. Sci.* **2016**, *9*, 3221.
(34) Han, J. H.; Khoo, E.; Bai, P.; Bazant, M. Z. *Sci. Rep.* **2014**, *4*, 7056.
(35) Schaefer, J. L.; et al. *J. Mater. Chem.* **2011**, *21*, 10094–10101.
(36) Kang, S. J.; et al. *J. Mater. Chem. A* **2014**, *2*, 9970–9974.
(37) Wright, W. W.; Hallden-Abberton, M. Polyimides. *Ullmann's Encyclopedia of Industrial Chemistry*; Wiley-VCH Verlag GmbH & Co. KGaA, 2000.

DOI: 10.1021/jacs.6b08730
J. Am. Chem. Soc. 2016, 138, 15443–15450

(38) Shin, S.; et al. *Nano Lett.* **2014**, *14*, 4395−4399.
(39) Hamilton, B. D.; Ha, J.; Hillmyer, M. A.; Ward, M. D. *Acc. Chem. Res.* **2012**, *45*, 414−423.
(40) Yamaki, J.; et al. *J. Power Sources* **1998**, *74*, 219−227.
(41) Tikekar, M. D.; Archer, L. A.; Koch, D. L. *J. Electrochem. Soc.* **2014**, *161*, A847−A855.
(42) Chazalviel, J. N. *Phys. Rev. A: At., Mol., Opt. Phys.* **1990**, *42*, 7355.
(43) Rosso, M. T.; et al. *J. Power Sources* **2001**, *97*−*98*, 804−806.
(44) Teyssot, A.; et al. *J. Electroanal. Chem.* **2005**, *584*, 70−74.
(45) Chang, H. J.; et al. *J. Am. Chem. Soc.* **2015**, *137*, 15209−15216.
(46) Bhattacharyya, R.; et al. *Nat. Mater.* **2010**, *9*, 504−510.
(47) Chandrashekar, S.; et al. *Nat. Mater.* **2012**, *11*, 311−315.
(48) Schweikert, N.; Hahn, H.; Indris, S. *Phys. Chem. Chem. Phys.* **2011**, *13*, 6234−6240.

DOI: 10.1021/jacs.6b08730
J. Am. Chem. Soc. 2016, 138, 15443−15450